City, University of London Institutional Repository

This is the accepted version of the paper.

This version of the publication may differ from the final published version.

1 Title page

2

3 Modelling of thrombin generation under flow in realistic left anterior

4 descending geometries

5

6

7

8

9

10

11 Dr Konstantinos P. Papadopoulos, City University London

12 Prof. Manolis Gavaises, City University London

13 Dr Grigoris T. Gerotziafas, Pierre and Marie Curie University- Paris 6

14

15

16

17 Corresponding author: Dr Konstantinos P. Papadopoulos
18 Email: Konstantinos.Papadopoulos.1@city.ac.uk, costis.papa@gmail.com

19 Telephone: +44 (0) 7580564404/ +30 6973498714

20 Fax: +44 207 040 8101
21
22 Address: City University London
23   SEMS
24   EC1V 0HB
25   Northampton square
26   London
27   United Kingdom
28

29

Abstract

31 Currently there are no available methods for prediction of thrombotic complications in

32 Coronary Artery disease. Additionally, blood coagulation tests are mainly performed in a

33 steady system while coagulation in vivo occurs under flow conditions. In this work, a

34 phenomenological model for coagulation up-to thrombin generation is proposed; the model

35 is mainly based on the results of thrombin generation assays and therefore it can account

36 for the variation of the coagulability that is observed in different individuals. The model is

37 applied on 3 cases of left anterior descending arteries (LAD) with 50% maximum stenosis

38 placed at a different location and have been statistically assessed as of different

39 complication risk. The simulations showed that parameters of thrombin generation assays

40 obtain different values when they refer to thrombin generation under realistic coronary flow

41 conditions. The flow conditions prevailing locally because of the geometric differences

42 among the arterial trees can lead to different initiation times and thrombin production rates

43 and it also alters the spatial distribution of the coagulation products. Similarly, small changes

44 of the coagulation characteristics of blood under identical flow conditions can allow or

45 prevent the initiation of coagulation. The results indicate that combined consideration of

46 geometry and coagulation characteristics of blood can lead to entirely different conclusions

47 compared to independent assessment of each factor.

Introduction

49 Coronary artery disease (CAD) is the formation of plaques in the interior of the coronary

50 vessel walls. This condition often leads to thrombus related complications that make CAD

51 the leading cause or mortality worldwide [1]. Thrombus formation in coronary artery . is

52 believed to be triggered by the rupture of an atheromatous plaque and subsequent

53 exposure of tissue factor (TF) and collagen. The triggering is followed by a series of

54　biochemical reactions that result in the activation of fibrin by thrombin and the formation of

55　the clot that narrows or blocks the flow in the coronary artery. As some of these reactions

56　occur much faster on the membrane of platelets and endothelium cells the contemporary

57　description of the process is cell-based[7]. Intracoronary ultrasound findings have suggested

58　that a ruptured plaque does not necessary lead to thrombosis [3-5]. This can be attributed to

59　any of the three factors, traditionally known as Virchow's triad, that influence the process:

60　(1) specific conditions on vessel's wall (2) coagulability of blood and (3) local flow conditions

61　[2].

62　. During the last three decades, there were several attempts to investigate aspects of the

63　process of thrombus formation using computational simulations. Based on in-vitro

64　experiments on the enzymatic reactions (indicatively[12]) zero-dimensional models that

65　reproduce the temporal evolution of the coagulation system have been developed., The first

66　model consisted of 14 reaction rate constants, describing the activation and inhibition of

67　four coagulation factors [13], while following works included up to 50 constants and focused

68　on the extrinsic [14, 15] or the intrinsic [16] pathway. Such models were used to investigate

69　specific parts of the coagulation process, as the function of positive feedback loops and

70　threshold concentrations for the initiation of the process [17], the triggering threshold with

71　respect to Tissue Factor Pathway Inhibitor (TFPI) concentration [18], the inhibition

72　mechanism of APC [19] or the effect of stochastically induced small variation of enzymes

73　concentration [20]. For the simulation of thrombus formation the temporal evolution of the

74　process is coupled with the diffusion and transport of the substances, initially as fluxes or

75　with the use of few reactions [21, 22]. The model of Sorensen et al, although focused on

76　platelet aggregation, could also fit into this category [23]. While there are recent works using

77　simplified reaction models, [24]. the trend is towards more complicated multi-scale and

78　multi-phase models. These models, in addition to the set of equations that represents the

79　reactions, may incorporate the movement of cells, the localization of equations and the

80 change of blood properties due to blood clotting. Kuharsky and Fogelson [25] proposed an

81 integrated model for thrombin generation under a simplified flow field, using a system of 59

82 equations that also included the binding of substances and the localization of reactions on

83 surfaces. . In following publications by the same group additional processes were

84 incorporated in the model:the alteration of the rheological properties of blood due to

85 clotting, by modelling platelet-platelet and platelet-wall interaction as reversible elastic

86 links. [26]. ;the APC mechanism and the transport of substances between plasma and

87 endothelium cells [27]. Additionally, a small scale discrete model using an immersed

88 boundary method [28] for platelets was utilized to develop a continuous model for platelet

89 aggregation

90   [29]; the later was also applied in simulations with pulsating flow in an idealized two

91 dimensional vessel bifurcation [30] and with the inclusion of transport within the thrombus,

92 was used to demonstrate the effects of flow conditions and the quantity of TF exposed on

93 thrombus growth [31]. A similar model was presented by Xu et al [32], which later included a

94 cellular pot model [33] for discrete cells and an energy-based stochastic process for cell

95 motion. The simulation involved differentiation of cell movements depending on fibrin levels

96 and cell-cell or cell-surface interaction and bonds. The model was used to evaluate the role

97 of fVII in venous thrombus formation [34] and to examine the impact of pulsating flow and

98 the non-Newtonian characteristics of blood on thrombus growth [35]. Anand et al [36]

99 presented another multi-process model that used a viscoelastic model to simulate flow for

100 both free vessel lumen and clot. This model also incorporated the activation of platelets due

101 to excessive shear stress and fibrin production and lysis. In a similar work, a model for the

102 viscosity of blood depending on fibrin concentration was proposed and used in a three-

103 dimensional simulation of blood coagulation in a tube [37].

104   For the case of coronary thrombosis, a typical value for the diameter of the artery is around

105   4mm and the flow is strongly three-dimensional and time dependent, preventing utilization

106   of simplified flow fields. Additionally there is significant variability of the response of the

107   coagulation system observed for different individuals [38]. From the reviewed works, only

108   the latest was applied on 3D geometries, while the typical used regions are 2D simplified

109   geometries with dimensions of $100 \times 100 \mu m^2$.In most studies the flow field is simplified and

110   predefined. Finally, the inclusion of a large number of processes makes the application of

111   the models computationally expensive while at the same time they require a large amount

112   of experimental data in order to be adapted for different patients. Due to these limitations

113   of the existing methods there is no connection between modelling of thrombus formation

114   and clinical practice.

115   In this work, we propose a model for coagulation under realistic flow conditions up to the

116   stage of thrombin generation that compensates for some of these difficulties. The proposed

117   phenomenological model has the following characteristics: (1) computational effectiveness,

118   so that it can be coupled with transient flow simulations; (2) ability to obtain patient specific

119   character in a manner that can be directly related to clinical practice, drawing data directly

120   from clinical tests.

Materials and methods

121

Thrombus modelling

122

123   For the description of the coagulation process the cell based approach (Figure 1) was

124   followed. The computational model was realized in three steps: (i) a zero dimensional sub-

125   model for thrombin generation was developed; (ii) the thrombin-sub model was modified

126   for application under flow and (iii) a sub-model for platelet aggregation under flow was

127   added. For the simulation of the coagulation reactions up to thrombin generation our

128   previously published phenomenological model was used [39], consisting of the 4-lumped

equations of Table 1. These equations express the concentration of 4 species in a zero-

dimensional system. The outcome is the temporal evolution of thrombin concentration. The

reaction rate constants of the model are derived directly from thrombin generation assays

and can be adjusted within a reasonable range in order to reproduce the results of thrombin

generation assays for a wide range of cases including haemophilia. The adjustment can be

performed either manually or via a repetitive algorithm.

Thrombin	$[IIa]$	$-k_{in,0}[IIa] + \left(k_{II}^{AP} \cdot \left[AP^{(f)}\right]\right) \cdot [II]$
Prothrombin	$[II]$	$-\left(k_{II}^{AP} \cdot \left[AP^{(f)}\right]\right) \cdot [II]$
Resting platelets in flow	$[RP^{(f)}]$	$-\left(k_{AP}^{IIa} + k_{AP}^{AP} \cdot \left[AP^{(f)}\right]\right) \cdot \left[RP^{(f)}\right]$
Activated platelets in flow	$[AP^{(f)}]$	$+\left(k_{AP}^{IIa} + k_{AP}^{AP} \cdot \left[AP^{(f)}\right]\right) \cdot \left[RP^{(f)}\right]$

Table 1: Lumped reactions of the thrombin generation submodel for the blood
circulating species.

The described physical system corresponds to a well-mixed solution, where the spatial

distributions of the concentration of all species are uniform. At the same time each of the

reactions and the respective reaction rates correspond to processes occurring either in

plasma, on the membrane of activated platelets or at the sites where TF is expressed

according to the cell based approach [7]. This is achieved with the use of different reaction

rate constants for the areas with activated platelets and the additional reaction terms for

the areas near the reacting vessel surface.

$[IIa]$		$-k_{in,add}[IIa] + (k_{TF,surf} + k_{II}^{AP}[AP^{(b)}])[II]$
$[II]$		$-(k_{TF,surf} + k_{II}^{AP}[AP^{(b)}])[II]$
$[RP^{(f)}]$	**bind**	$-\left(\left(k_{bi,surf}^{RP} \cdot A_f + k_{bi,RP}^{RP} \cdot [RP^{(b)}] + k_{bi,AP}^{RP} \cdot [AP^{(b)}]\right) \cdot \left[RP^{(f)}\right]\right)$
	act	$- k_{AP}^{AP} \cdot \left[AP^{(b)}\right] \cdot \left[RP^{(f)}\right]$
$[AP^{(f)}]$	**bind**	$-\left(\left(k_{bi,surf}^{AP} \cdot A_f + k_{bi,RP}^{AP} \cdot [RP^{(b)}] + k_{bi,AP}^{AP} \cdot [AP^{(b)}]\right) \cdot \left[AP^{(f)}\right]\right)$
	act	$+ k_{AP}^{AP} \cdot \left[AP^{(b)}\right] \cdot \left[RP^{(f)}\right]$

$[\boldsymbol{RP^{(b)}}]$	**bind**	$+\left(\left(k_{bi,surf}^{RP}\cdot A_f + k_{bi,RP}^{RP}\cdot[RP^{(b)}] + k_{bi,AP}^{RP}\cdot[AP^{(b)}]\right)\cdot[RP^{(f)}]\right) - k_{diss}^{RP}[RP^{(b)}]^2$
	act	$-\ k_{AP}^{IIa}[RP^{(b)}] - k_{AP}^{AP}([AP^{(b)}] + [AP^{(f)}])\cdot[RP^{(f)}] - k_{AP}^{surf}[RP^{(b)}]$
$[\boldsymbol{AP^{(b)}}]$	**bind**	$+\left(\left(k_{bi,surf}^{AP}\cdot A_f + k_{bi,RP}^{AP}\cdot[RP^{(b)}] + k_{bi,AP}^{AP}\cdot[AP^{(b)}]\right)\cdot[RP^{(f)}]\right) - k_{diss}^{AP}[AP^{(b)}]^2$
	act	$+\ k_{AP}^{IIa}[RP^{(b)}] - k_{AP}^{AP}\cdot([AP^{(b)}] + [AP^{(f)}])\cdot[RP^{(f)}] + k_{AP}^{surf}[RP^{(b)}]$

144 Table 2: The additional reaction terms in the computational cells attached to the
145 reacting part of the vessel wall. They describe the activation (act) and binding (bind)
146 of platelets and the additional thrombin generation due to surface TF exposure and
147 bound activated platelets. Each reaction rate constant of the form k_B^A simulates the
148 effect of substance B on the concentration of A.

149 .

150 Coupling with flow

151 For the simulations including flow, the concentrations $(C_i{}^{(f)})$ of the blood circulating species

152 were calculated using the convection-diffusion equation with source terms (S_i) (equation 1).

153 For immobilized species $(C_j{}^{(b)})$ the source term expresses the temporal evolution (equation

154 2).

$$\frac{\partial C_i{}^{(f)}}{\partial t} + \nabla\left(C_i{}^{(f)}\cdot\vec{u}\right) = D\nabla^2 C_i{}^{(f)} + S_i$$

155   Equation 1

$$\frac{\partial C_j{}^{(b)}}{\partial t} = S_j$$

156   Equation 2

157 The quantity of bound species is expressed in surface concentration (kg/m^2), while the

158 circulating species in volume concentration (kg/kg). In the reactions involving transition of a

159 species from circulating to bound state and vice versa the actual mass of the involved

160 species in the computational cell is calculated, using the volume of the computational cell or

161 the reacting surface. Then the fraction of the species that is binding or unbinding is

162 computed using the appropriate reaction rate constant.

7

163   During in vivo coagulation, TF is located on the vessel wall during initiation and therefore the

164   bulk initiation reaction used in the thrombin sub-model needs to be replaced by a surface

165   reaction. In order to obtain a value for this surface reaction we exploited the experimental

166   results of Shen et al [40] regarding the threshold behaviour of coagulation initiation under

167   flow. This study revealed that the initiation of coagulation under flow occurs only when the

168   stream-wise length of the reacting surface is sufficiently large and the wall shear rate is

169   sufficiently low. We simulated the described experimental cases (Figure 2) and we adjusted

170   the surface reaction rate constant to achieve initiation of coagulation for the above-

171   threshold experimental setups and at the same time not to have initiation for the below-

172   threshold setups.

173   The platelet aggregation sub-model was developed based on the results of Badimon et al

174   [41] regarding the binding of platelets on de-endothelized vessel stripes under flow. The

175   experimental setup was reconstructed and three cases with different wall shear rate values

176   were simulated (Figure 3) as described in the experiment. The aggregation rate constant

177   used for the platelets was shear-dependent and for the specific part there was no distinction

178   between resting and activated platelets.

179   As the proposed coagulation model is phenomenological, each of the used reactions stands

180   for a number of actual processes. The outcome of the model is the temporal evolution of

181   thrombin generation. 'Prothrombin' in the sense used in the model represents the coagulant

182   potential of blood. In the same manner, the surface initiation reaction incorporates all the

183   processes that intervene between the expression of TF and the activation of thrombin.

184   Similarly, the activated platelets account for all the additional activity involved in the

185   amplification phase.

Geometry reconstruction

186 Finally, the developed model was applied in realistic LAD geometries under flow conditions.

188 Three different geometrical models, MI1, MI2 and STA with maximum radius reduction 50%,

189 were constructed [42] using the centrelines and the diameters of the vessels as obtained

190 from coronary angiographies. The geometries have been previously assessed as of different

191 complication risk [43] based on statistical correlation of the occurrence of acute coronary

192 syndromes to the location of the stenosis and the existence of bifurcations within the

193 affected lesion. In the STA geometry there are no bifurcations involved in the stenotic lesion

194 and it is considered of low complication risk while in MI1 and MI2 geometries there are

195 bifurcations within the stenotic lesion and they are considered of higher risk regarding acute

196 coronary complications [44]. A reacting area of 6mm stream-wise length was defined on

197 each of the three geometries with the centre of the reacting area being at the point of

198 maximum radius reduction (Figure 4).The transient flow field for one cardiac cycle was

199 obtained using CFD techniques [42].

Flow field

201 For the velocity $\vec{u}$ at each point a predefined time dependent value was used in all

202 simulations. The flow field was calculated by solving the incompressible Navier-Stokes

203 equations with the use of the commercial software ANSYS FLUENT and the details have been

204 previously published [42, 45]. In brief, blood was modelled as a single-phase Newtonian fluid

205 with density 1060kg/m^3 and viscosity $3.5 \cdot 10^{-3} Pa \cdot s$. Aortic pressure pulse was applied at

206 the inlet of the geometry and outflow resistance boundary conditions at the outlets. The

207 time scale of the cardiac cycle is of the order of 1s, approximately 5000 times smaller

208 compared to the timescale of the coagulation model. As the model is mainly sensitive to the

209 wall shear rate and it has been shown that wall shear mainly depends on the average flow

210 rate rather than the exact shape of the inlet pulse[46, 47], a simplified inflow pulse

211   consisting of 9 time instances of the original cardiac pulse was used. The total inflow of the

212   used pulse was 0.85% elevated, compared to the mass flow inlet of the initial pulse.

213   All the simulations were performed using an i7 intel processor in serial computing (single

214   core computations). Simulating the flow for three cardiac pulses lasted approximately one

215   day, while the application of the biochemical model under transient flow conditions required

216   approximately five days for simulating real time of some minutes.

217   ## Results

218   We started the simulations of the experiments of Shen et al [40] with an estimated value for

219   the reaction rate constant for the surface induced initiation, based on geometrical

220   assumptions. Using trial and error we approximated the surface initiation of the coagulation

221   with the value $k_{TF,surf} = 1.785 \cdot 10^{-6} \frac{kg}{m^2} \cdot s^{-1}$. This constant represents the thrombin

222   production rate from a surface where TF is expressed, per surface unit. Using this value for

223   the surface initiation reaction, the simulations for the above threshold experimental cases

224   resulted in initiation of the coagulation process, while in the simulations of the sub-

225   threshold setups the concentration of thrombin was found below the minimum value that

226   leads to platelet activation after 200s of perfusion (Figure 5), in accordance to the simulated

227   experiments [40].

228   A number of sub-threshold setups were also simulated to test the behaviour of the model

229   (Table 1). As the initiation was considered a surface reaction, the threshold condition for the

230   transition from the initiation to the amplification phase was also modified and was

231   expressed as amount of thrombin per surface unit $[IIa]_{th}^{(s)} = 3.44 \cdot 10^{-9} \cdot nmol/mm^2$

232   instead of being expressed as volume concentration (1.2nM). This modification implies that

233   the initiation occurs in a reaction zone of approximately 3μm above the reacting surface.

234   This approach also enforces the mesh independence of the model. As the surface thrombin

235   generation is proportional to the reacting surface, using a transition criterion based on the

10

volume concentration of thrombin would lead to strong dependence of the transition on the

volume of the computational cell. The simulations also revealed that from the wall shear

rate value (γ_w) and the stream-wise length of the reacting area (L_{SWR}), we can derive a

quantity, previously defined as coagulation activation index [42], $CAI = L_{SWR}/\gamma_w$ that is

related to the initiation of coagulation. CAI is proportional to the residence time of the blood

components over the reacting surface. As shown in Table 1, for a given value of $k_{TF,surf}$ a

small modification of the parameters can allow or prevent the initiation of coagulation,

depending on the change of CAI value.

Case	WSR (s^{-1})	L_{SWR}(m)	$k_{TF,surf}$	CAI $(10^{-5}m \times s)$	initiation
SA Basic case 1	25	$2 \cdot 10^{-4}$	$1.785 \cdot 10^{-6}$	0.8	YES
SB Basic case 2	40	$4 \cdot 10^{-4}$	$1.785 \cdot 10^{-6}$	1	YES
SA with lower reaction rate constant	25	$2 \cdot 10^{-4}$	$1.775 \cdot 10^{-6}$	0.8	NO
SA with elevated shear rate	30	$2 \cdot 10^{-4}$	$1.785 \cdot 10^{-6}$	0.625	NO
SB with elevated shear rate	60	$4 \cdot 10^{-4}$	$1.785 \cdot 10^{-6}$	0.667	NO

Table 3: The basic cases used for the calculation of the surface initiation reaction rate were SA and SB. SA was the case with minimum CAI and required the maximum value of $k_{TF,surf}$ for initiation. The following three cases as many others not presented were simulated in order to confirm that SA and SB were actually threshold setups for the initiation and that a small modification of the parameters to the direction of reduced CAI does not allow initiation.

The platelet aggregation model was tested for the three different flow conditions described

in the simulated experiment. The experimental results of platelet aggregation regarding the

maximum amount of bound platelets and the initial aggregation rate were accurately

approximated by the simulations as shown in Figure 6. The model failed to predict the

254   disaggregation of platelets that was observed in high shear rate conditions after 10 min of

255   perfusion. However this happens more likely due to stress accumulation as the aggregate is

256   continuously subject to high shear stress values ($1690s^{-1}$) while for the transient coronary

257   flow used in this study the average wall shear rate is much lower ($235s^{-1}$)**.**

258   For the two sets of simulations described above, the flow field was obtained by solving the

259   incompressible Navier-Stokes equations in FLUENT ANSYS, while fixed mass flowrates were

260   used for both the inlet and the outlet of computational domain. As the interaction between

261   flow and biochemical reactions is not considered, the biochemical models were applied on

262   steady predefined flow field.

263   For the simulations in the LAD geometries the setup of the coagulation model was identical,

264   with the processes regarding thrombin generation tuned in order to correspond to typical

265   values of TGA. For the simulations under flow we calculated the parameters of TGA: the lag

266   time (Tlag), the time until thrombin reaches its maximum concentration (ttP), the maximum

267   concentration of thrombin Cmax and the production rate of thrombin and as an additional

268   characteristic parameter of the simulations was considered the moment when thrombin

269   concentration exceeded the threshold value for the transition of coagulation from the

270   initiation to the amplification phase (1.2nM) at a point downstream the reacting site

271   (downstream propagation time or DP time). The values of these parameters for the TGA and

272   the three LAD models are summarized in Table 2. While all three models had similar

273   maximum values of thrombin concentration, the temporal evolution was different for each

274   model (Figure 7).

	Lag time (min)	Time to peak (min)	$C_{max}(nM)$	Production rate (nM/s)	DP time (min)
TGA	*3.6 ± 0.8*	*7.4±1.8*	*164±50*	*1*	*n/a*

STA	1	2	31	0.49	1.2
MI1	0.5	1.3	38	0.77	0.8
MI2	5	5.9	35	0.68	2.9

Table 4**: Influence of flow on thrombin generation parameters.** The values of the main parameters characterizing thrombin generation as calculated for the three LAD models compared to the standard TGA values.

In MI1 and STA geometries, the transition from initiation to amplification phase was fast and

levels of thrombin concentration that are considered sufficiently high to cause platelet

activation (>1.2nM) were present downstream the reacting area only after the amplification.

In these models the downstream propagation was observed after the initiation phase. In

MI2 geometry the process had much slower progress and while in specific points

downstream the reacting surface thrombin exceeds the threshold value during the initiation

phase. The simulations were stopped 2 minutes after the downstream propagation and after

maximum thrombin concentration had obtained a constant value, approximately 1.5

minutes after the downstream propagation. In all cases the process was limited in a small

zone near the vessel wall, even in the presence of vortices.

The difference in the temporal evolution is caused by the different distribution of bound

activated platelets on the reacting surface of the vessel wall (Figure 8). While the total

amount increases in a similar manner for all three geometries, in MI1 and STA geometry

there is a small area at the end of the reacting boundary where the amount of bound

activated platelets is more than one order of magnitude higher than the average. On the

contrary, in MI2 geometry activated platelets are uniformly distributed on the reacting

surface and this has as a result a prolonged initiation phase and a large amount of activated

platelets at the instance of the transition to the amplification phase. This large amount of

bound activated platelets in MI2 geometry explains the observation of above threshold

(>1.2nM) thrombin concentration before the main amplification phase.

Discussion

Application of the coagulation model under flow resulted in lower maximum concentration of thrombin compared to the TGA. The initiation time was also different than the TGA values, in MI1 and STA significantly smaller while in MI2 significantly larger. Thrombin generation rate though was similar for all cases and close to the TGA value (Table 2). As TGA parameters have absolute and not only comparative value, these findings indicate that the results of steady state coagulation tests should be somehow translated under flow conditions. Perfusion tests require a relatively large amount of blood and are difficult to standardize, therefore the easier way to correlate the results of steady state clinical tests to coagulation under flow is via computer simulations.

The results of the coagulation model on the different geometries highlight the importance of local flow conditions on the evolution of the process. The simulations were performed with identical setup of the coagulation model therefore all three cases assume identical behaviour of blood regarding coagulability. However, in MI2 case the temporal evolution was much slower and the local conditions at the moment of the transition from initiation to amplification phase were different, as thrombin concentration and amount of bound activated platelets were elevated compared to the other two cases. This shows that the coagulation tests provide only a part of the important information regarding the condition of a patient as similar results might lead to entirely different situations. Again, this can be assessed only in-silico, as any experiments or clinical tests are not feasible.

During the calibration of the model under flow conditions it became obvious that the initiation phase is very sensitive to the surface thrombin production rate and the local value of the wall shear. At first site this indicates that the exact concentration of TF in the atheromatous plaque may play an important role in the initiation and the transition to the amplification phase. However, the dependence of the initiation rate on TF concentration

323   according to experimental results [48] is logarithmic [42] so the actual reaction rate is not

324   that sensitive to small variations of TF concentration. As there is available information for

325   the surface concentration of TF on atheromatous plaques [49] an experiment similar to the

326   one performed by Shen et al [40] with known surface concentration of TF on the reacting

327   surface can lead to a value for this constant that will be appropriate for general use in the

328   cases when plaque rupture or vessel injury is assumed.

329   In MI2 case the prolonged initiation phase was combined with high concentration of bound

330   activated platelets in the reacting area. A prolonged lag phase of thrombin generation in a

331   thrombin generation assay is mainly related to hypocoagulable states. Increased lag time is

332   observed in cases with reduced stimulation or increased inhibition of thrombin [50]. On the

333   contrary, the application of the coagulation model under flow shows that a prolonged

334   initiation phase leads to increased accumulation of activated platelets at the reacting site.

335   These bound platelets will become activated during the propagation phase and contribute

336   locally to thrombin generation. The observed mechanism indicates that it is very possible

337   that the prolonged lag phase indicates increased risk for thrombotic complications in vivo,

338   provided that an initiation stimulus is present a fact that also supported by recent clinical

339   findings [51].

340   It is interesting to note that while flow seems to have an important role, the whole process

341   of coagulation in LAD models was limited into a small boundary layer near the vessel wall.

342   The concentration of thrombin and activated platelets becomes approximately zero in a

343   small distance from the vessel wall. As Peclet number is too high ($>10^4$) even in a small

344   distance (~3μm) from the vessel wall, diffusion was not expected to have significant role

345   under arterial flow conditions but the restriction of coagulation products near the wall

346   occurs also in the areas where vortices are present. Therefore, according to our findings the

347 more important aspect of flow for coagulation is wall shear rate, while the possible

348 contribution of recirculation zones to the process was not confirmed by this work.

349 As the main concept in this work is the correlation of coagulation models with clinical tests,

350 in the future we intent to modify the proposed mathematical model for coagulation in a

351 manner that the platelet aggregation sub-model will be also calibrated based on existing

352 clinical platelet assays. We also intend to add the fibrin activation and polymerization part of

353 the process and correlate the model with thromboelastography tests (TEG). Finally, we also

354 hope, through partnership with a biochemical lab, to achieve in vitro quantitative validation

355 of the method by performing perfusion tests in coronary models. However, the findings of

356 this study indicate that it would be useful for clinical practice to co-estimate the prevailing

357 flow conditions and blood coagulability for each patient, and that this co-estimation can be

358 performed via numerical simulations.

Conclusions

359

360 In this study we proposed a method for modelling coagulation under flow up to thrombin

361 generation, based partly on clinical tests. We demonstrated that it is feasible to build a

362 coagulation model based on clinical tests instead of laboratory experiments and therefore

363 achieve a patient specific and more importantly clinically relevant simulation of blood

364 coagulation. The application of the model revealed that certain parameters that characterize

365 thrombin generation in TGA tests obtain different values for thrombin generation under

366 realistic flow conditions. Additionally, we showed that identical behaviour of blood can lead

367 to different temporal evolution of coagulation depending on the geometry of the coronary

368 and the flow conditions. As experiments in-vivo on coronary thrombosis are not feasible and

369 relative measurements are also extremely limited, the findings of this study demonstrate

370 that mathematical simulation of coagulation in a case specific manner is a promising and

371   inexpensive pathway towards the assessment of coronary disease and can contribute to the

372   prognosis of thrombotic complications.

373   **Conflicts of interest**

374   None.

375   **Funding:**

376   Part of this work was funded by EPSRC, as a PhD scholarship

377   **Ethical approval:** not required

378

379   References

380   [1] Roger VL, Go AS, Lloyd-Jones DM, Adams RJ, Berry JD, Brown TM, et al. Heart disease and
381   stroke statistics--2011 update: a report from the American Heart Association. Circulation.
382   2011;123:e18-e209.
383   [2] Lee KW, Lip GY. Acute coronary syndromes: Virchow's triad revisited. Blood coagulation
384   & fibrinolysis. 2003;14:605-25.
385   [3] Hong MK, Mintz GS, Lee CW, Kim YH, Lee SW, Song JM, et al. Comparison of coronary
386   plaque rupture between stable angina and acute myocardial infarction: a three-vessel
387   intravascular ultrasound study in 235 patients. Circulation. 2004;110:928-33.
388   [4] Maehara A, Mintz GS, Bui AB, Walter OR, Castagna MT, Canos D, et al. Morphologic and
389   angiographic features of coronary plaque rupture detected by intravascular ultrasound.
390   Journal of the American College of Cardiology. 2002;40:904-10.
391   [5] Rioufol G, Finet G, Ginon I, Andre-Fouet X, Rossi R, Vialle E, et al. Multiple atherosclerotic
392   plaque rupture in acute coronary syndrome: a three-vessel intravascular ultrasound study.
393   Circulation. 2002;106:804-8.
394   [6] Heemskerk JW, Bevers EM, Lindhout T. Platelet activation and blood coagulation.
395   THROMBOSIS AND HAEMOSTASIS-STUTTGART-. 2002;88:186-94.
396   [7] Smith SA. The cell-based model of coagulation. Journal of Veterinary Emergency and
397   Critical Care. 2009;19:3-10.
398   [8] Hathcock JJ. Flow Effects on Coagulation and Thrombosis. Arteriosclerosis, Thrombosis,
399   and Vascular Biology. 2006;26:1729-37.
400   [9] Nesbitt WS, Westein E, Tovar-Lopez FJ, Tolouei E, Mitchell A, Fu J, et al. A shear gradient-
401   dependent platelet aggregation mechanism drives thrombus formation. Natural Medicines.
402   2009;15:665-73.
403   [10] Yin W, Shanmugavelayudam SK, Rubenstein DA. The effect of physiologically relevant
404   dynamic shear stress on platelet and endothelial cell activation. Thrombosis Research.
405   2011;127:235-41.
406   [11] Goto S, Ikeda Y, Saldívar E, Ruggeri ZM. Distinct mechanisms of platelet aggregation as a
407   consequence of different shearing flow conditions. Journal of Clinical Investigation.
408   1998;101:479-86.
409   [12] Lawson JH, Kalafatis M, Stram S, Mann KG. A model for the tissue factor pathway to
410   thrombin. I. An empirical study. Journal of Biological Chemistry. 1994;269:23357-66.
411   [13] Willems G, Lindhout T, Hermens WT, Hemker H. Simulation Model for Thrombin
412   Generation in Plasma. Pathophysiology of Haemostasis and Thrombosis. 1991;21:197-207.
413   [14] Jones KC, Mann KG. A model for the tissue factor pathway to thrombin. II. A
414   mathematical simulation. Journal of Biological Chemistry. 1994;269:23367-73.
415   [15] Hockin MF, Jones KC, Everse SJ, Mann KG. A Model for the Stoichiometric Regulation of
416   Blood Coagulation. Journal of Biological Chemistry. 2002;277:18322-33.
417   [16] Zarnitsina VI, Pokhilko AV, Ataullakhanov FI. A Mathematical model for the spatio-
418   temporal dynamics of intrinsic pathway of blood coagulation. I. The model description.
419   Thrombosis Research. 1996;84:225-36.
420   [17] Beltrami E, Jesty J. Mathematical analysis of activation thresholds in enzyme-catalyzed
421   positive feedbacks: application to the feedbacks of blood coagulation. Proceedings of the
422   National Academy of Sciences. 1995;92:8744-8.
423   [18] Xu C, Hu Xu X, Zeng Y, Wen Chen Y. Simulation of a mathematical model of the role of
424   the TFPI in the extrinsic pathway of coagulation. Computers in Biology and Medicine.
425   2005;35:435-45.

426 [19] Qiao YH, Xu CQ, Zeng YJ, Xu XH, Zhao H, Xu H. The kinetic model and simulation of blood
427 coagulation--the kinetic influence of activated protein C. Medical Engineering & Physics
428 2004;26:341-7.
429 [20] Lo K, Denney WS, Diamond SL. Stochastic Modeling of Blood Coagulation Initiation.
430 Pathophysiology of Haemostasis and Thrombosis. 2005;34:80-90.
431 [21] Hubbell JA, McIntire LV. Platelet active concentration profiles near growing thrombi. A
432 mathematical consideration. Biophysical Journal. 1986;50:937-45.
433 [22] Folie BJ, McIntire LV. Mathematical analysis of mural thrombogenesis. Concentration
434 profiles of platelet-activating agents and effects of viscous shear flow. Biophysical Journal.
435 1989;56:1121-41.
436 [23] Sorensen EN, Burgreen GW, Wagner WR, Antaki JF. Computational Simulation of
437 Platelet Deposition and Activation: I. Model Development and Properties. Annals of
438 Biomedical Engineering. 1999;27:436-48.
439 [24] Lobanov AI, Starozhilova TK. The Effect of Convective Flows on Blood Coagulation
440 Processes. Pathophysiology of Haemostasis and Thrombosis. 2005;34:121-34.
441 [25] Kuharsky AL, Fogelson AL. Surface-Mediated Control of Blood Coagulation: The Role of
442 Binding Site Densities and Platelet Deposition. Biophysical Journal. 2001;80:1050-74.
443 [26] Fogelson AL, Guy RD. Platelet–wall interactions in continuum models of platelet
444 thrombosis: formulation and numerical solution. Mathematical Medicine and Biology.
445 2004;21:293-334.
446 [27] Fogelson AL, Tania N. Coagulation under Flow: The Influence of Flow-Mediated
447 Transport on the Initiation and Inhibition of Coagulation. Pathophysiology of Haemostasis
448 and Thrombosis. 2005;34:91-108.
449 [28] Peskin CS. The immersed boundary method. Acta Numerica. 2002;11:479-517.
450 [29] Fogelson AL, Guy RD. Immersed-boundary-type models of intravascular platelet
451 aggregation. Computer Methods in Applied Mechanics and Engineering. 2008;197:2087-104.
452 [30] Yang XS, Lewis RW, Zhang HY. Finite Element Analysis of Fogelson's Model for Platelet
453 Aggregation. 2004.
454 [31] Leiderman K, Fogelson AL. Grow with the flow: a spatial–temporal model of platelet
455 deposition and blood coagulation under flow. Mathematical Medicine and Biology.
456 2011;28:47-84.
457 [32] Xu Z, Chen N, Kamocka MM, Rosen ED, Alber M. A multiscale model of thrombus
458 development. Journal of The Royal Society Interface. 2008;5:705-22.
459 [33] Marée AM, Grieneisen V, Hogeweg P. The Cellular Potts Model and Biophysical
460 Properties of Cells, Tissues and Morphogenesis. In: Anderson AA, Chaplain MJ, Rejniak K,
461 editors. Single-Cell-Based Models in Biology and Medicine: Birkhäuser Basel; 2007. p. 107-
462 36.
463 [34] Xu Z, Lioi J, Mu J, Kamocka MM, Liu X, Chen DZ, et al. A Multiscale Model of Venous
464 Thrombus Formation with Surface-Mediated Control of Blood Coagulation Cascade.
465 Biophysical Journal. 2010;98:1723-32.
466 [35] Xu Z, Chen N, Shadden SC, Marsden JE, Kamocka MM, Rosen ED, et al. Study of blood
467 flow impact on growth of thrombi using a multiscale model. Soft Matter. 2009;5:769-79.
468 [36] Anand M, Rajagopal K, Rajagopal KR. A Model for the Formation and Lysis of Blood
469 Clots. Pathophysiology of Haemostasis and Thrombosis. 2005;34:109-20.
470 [37] Bodnár T, Sequeira A. Numerical simulation of the coagulation dynamics of blood.
471 Computational and Mathematical Methods in Medicine. 2008;9:83-104.
472 [38] Oliver JA, Monroe DM, Roberts HR, Hoffman M. Thrombin Activates Factor XI on
473 Activated Platelets in the Absence of Factor XII. Arteriosclerosis, Thrombosis, and Vascular
474 Biology. 1999;19:170-7.

475 [39] Papadopoulos KP, Gavaises M, Atkin C. A simplified mathematical model for thrombin
476 generation. Medical Engineering & Physics. 2014;36:196-204.

477 [40] Shen F, Kastrup CJ, Liu Y, Ismagilov RF. Threshold Response of Initiation of Blood
478 Coagulation by Tissue Factor in Patterned Microfluidic Capillaries Is Controlled by Shear
479 Rate. Arteriosclerosis, Thrombosis, and Vascular Biology. 2008;28:2035-41.

480 [41] Badimon L, Badimon JJ, Galvez A, Chesebro JH, Fuster V. Influence of arterial damage
481 and wall shear rate on platelet deposition. Ex vivo study in a swine model. Arteriosclerosis,
482 Thrombosis, and Vascular Biology. 1986;6:312-20.

483 [42] Papadopoulos KP. Flow effect on thrombus formation in stenosed coronary arteries: a
484 computational study: City University London; 2015.

485 [43] Katritsis DG, Pantos J, Efstathopoulos E. Hemodynamic factors and atheromatic plaque
486 rupture in the coronary arteries: from vulnerable plaque to vulnerable coronary segment.
487 Coronary Artery Disease. 2007;18:229-37.

488 [44] Katritsis DG, Efstathopoulos EP, Pantos J, Korovesis S, Kourlaba G, Kazantzidis S, et al.
489 Anatomic Characteristics of Culprit Sites in Acute Coronary Syndromes. Journal of
490 Interventional Cardiology. 2008;21:140-50.

491 [45] Papadopoulos KP, Gavaises M, Pantos I, Katritsis DG, Mitroglou N. Derivation of flow
492 related risk indices for stenosed left anterior descending coronary arteries with the use of
493 computer simulations. Medical Engineering & Physics.

494 [46] Johnston BMJaPR. Simulations of pulsatile blood flow in tapered S-shaped in-plane and
495 out-of-plane coronary arteries. 18th World IMACS / MODSIM Congress, Cairns, Australia.
496 2009.

497 [47] Myers JG, Moore JA, Ojha M, Johnston KW, Ethier CR. Factors Influencing Blood Flow
498 Patterns in the Human Right Coronary Artery. Annals of Biomedical Engineering.
499 2001;29:109-20.

500 [48] Gerotziafas GT, Depasse F, Busson J, Leflem L, Elalamy I, Samama MM. Towards a
501 standardization of thrombin generation assessment: The influence of tissue factor, platelets
502 and phospholipids concentration on the normal values of Thrombogram-Trombinoscope
503 assay. Thrombosis Journal. 2005;3.

504 [49] Bonderman D, Teml A, Jakowitsch J, Adlbrecht C, Gyöngyösi M, Sperker W, et al.
505 Coronary no-reflow is caused by shedding of active tissue factor from dissected
506 atherosclerotic plaque. Blood. 2002;99:2794-800.

507 [50] Castoldi E, Rosing J. Thrombin generation tests. Thrombosis Research. 2011;127,
508 Supplement 3:S21-S5.

509 [51] Smid M, Dielis A, Winkens M, Spronk H, Van Oerle R, Hamulyak K, et al. Thrombin
510 generation in patients with a first acute myocardial infarction. Journal of Thrombosis and
511 Haemostasis. 2011;9:450-6.

512

513 Figure captions

514 Figure 1: **Phenomenological thrombin generation model.** The simplified cell based concept

515 used for the development and application of the thrombin sub-model under flow. The

516 different colours of arrows indicate the processes that are lumped in each reaction rate

517 constant used. K_{in}: Thrombin inhibiton; k_{AP}^{IIa}:Activation of platelets by thrombin; k_{II}^{AP}:

518 Thrombin activation due to activated platelets; k_{TF}; Initiation by exposed TF k_{AP}^{AP}: Activation

519 of platelets due to the presence of activated platelets

520 Figure 2: **Surface initiation simulations.** The experimental setup of the two basic cases used

521 for the calculation of the rate constant for the surface initiation reaction. The length

522 upstream the TF bearing surface was sufficiently long in order for a parabolic velocity profile

523 to be developed.

524 Figure 3: **Platelet aggregation simulations.** The geometry and the flow parameters used for

525 the calibration and validation of platelet aggregation sub model

526 Figure 4: **Figure 4**: **Location of reacting lesion in coronary models.** The three LAD models

527 used for the application of the thrombus formation, MI1 MI2 and STA. The maximum

528 stenosis was 50% radius reduction compared to the health LAD model. The stream-wise

529 length of the reacting surface is 6mm in all cases and the centre of the reacting area is at the

530 peak of the stenosis.

531 Figure 5: **Above threshold vs sub-threshold setup.** Comparison of an above threshold (up)

532 and a sub-threshold (down) setup regarding the initiation of coagulation. In the above

533 threshold setup, the concentration of thrombin is increasing downstream the reacting

534 surface and is sufficiently high (>1nM) to cause platelet activation and the results

535 correspond to 120s perfusion time.

536 Figure 6: **Platelet aggregation for different shear rates.** The performance of the platelet

537 aggregation sub-model. The simulations follow the experimental results regarding the initial

538 deposition rate and the maximum deposition. For the case with high shear rate the model

539 fails to reproduce the disaggregation of the platelets after 10min of perfusion. However, in

540 this case both perfusion time and wall shear rate are extremely high compared to the

541   conditions of simulations in LAD geometries (t <6mins and $\gamma_w \approx 240 s^{-1}$). The dashed line

542   corresponds to the full surface coverage.

543   Figure 7: **Maximum thrombin concentration.** Temporal evolution of maximum thrombin

544   concentration for the three LAD models. For all models maximum thrombin concentration is

545   approximately 25% of the TGA value. For MI1 and STA the initiation phase is significantly

546   short while for MI2 case is long compared to TGA.

547
548
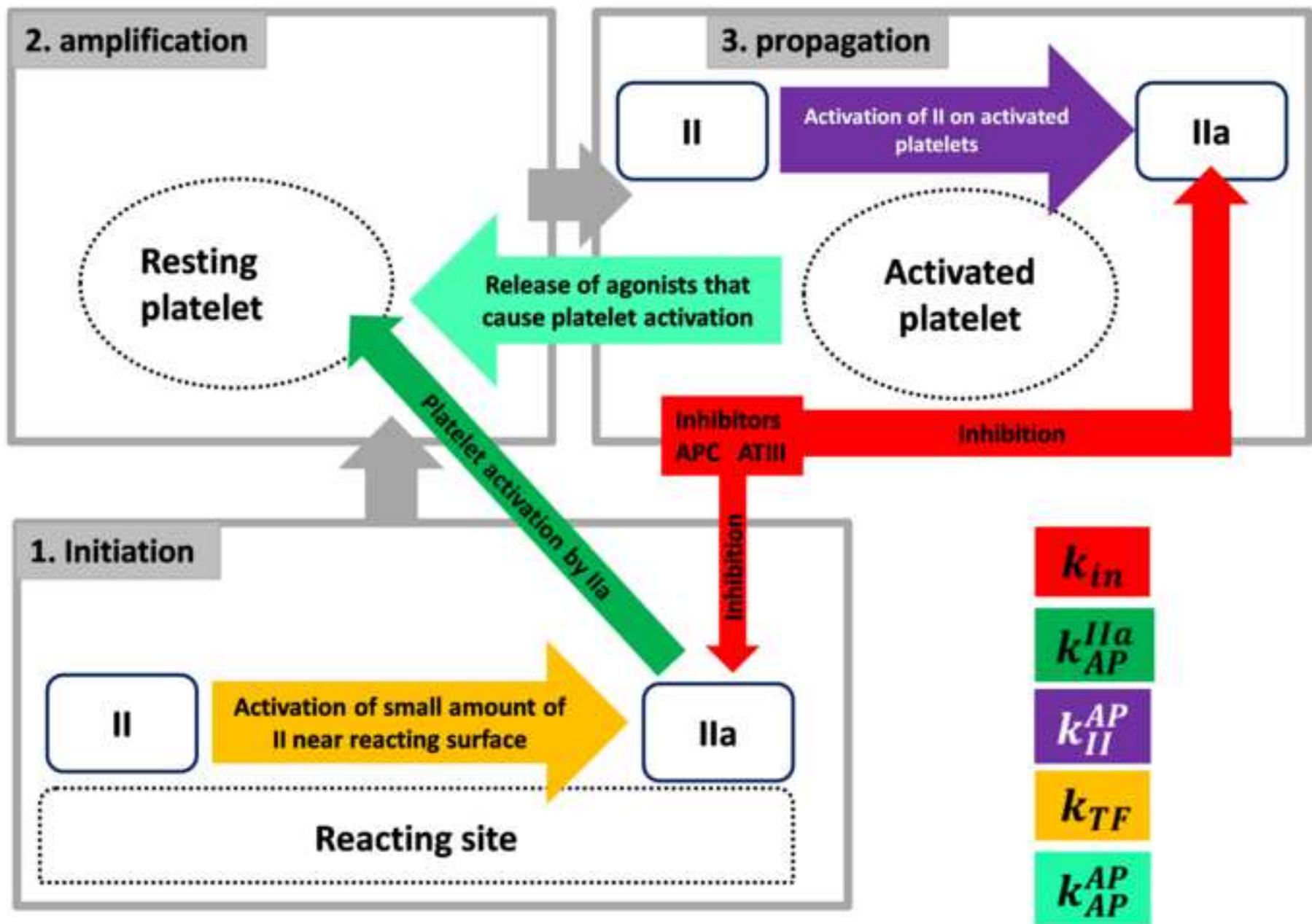
Length	2mm
Diameter	0.45mm
RW length	0.2mm
Shear	$25s^{-1}$
Mass flow	$2.37 \cdot 10^{-7}$ kg/s

Length	2mm
Diameter	0.45mm
RW length	0.4mm
Shear	$40s^{-1}$
Mass flow	$3.70 \cdot 10^{-7}$ kg/s

Velocity profile upstream the reacting wall

Reacting wall
(de-endothelized vessel segments)

0.012

U(m/s)

0

	Simulated Cases	
Case	Shear rate (s^{-1})	Inlet mass flow (kg./s)
PLA1	106	$8.825 \cdot 10^{-5}$
PLA2	212	$1.765 \cdot 10^{-4}$
PLA3	1690	$1.407 \cdot 10^{-3}$

MI1   MI2   STA

Reacting site of 6mm stream-wise length
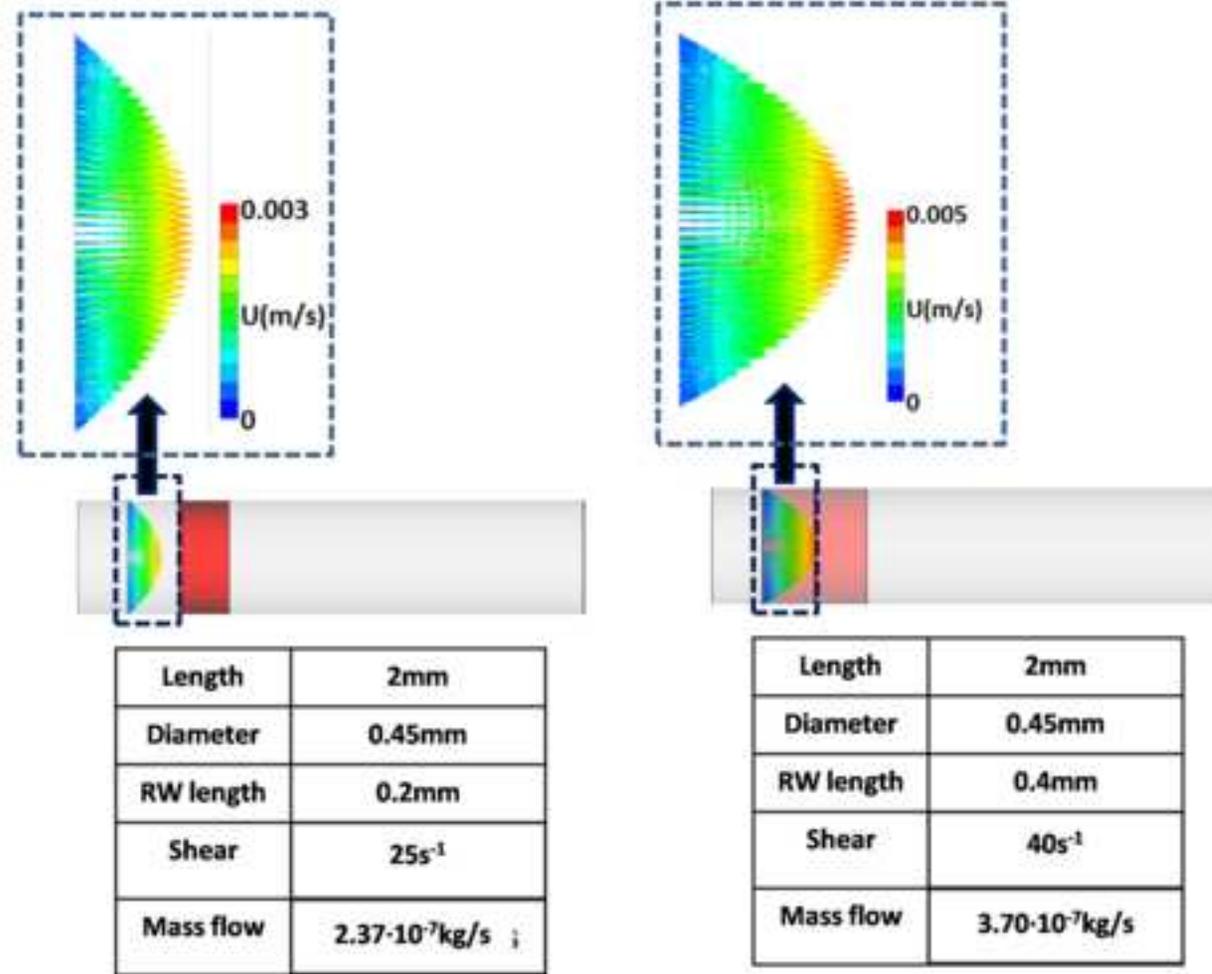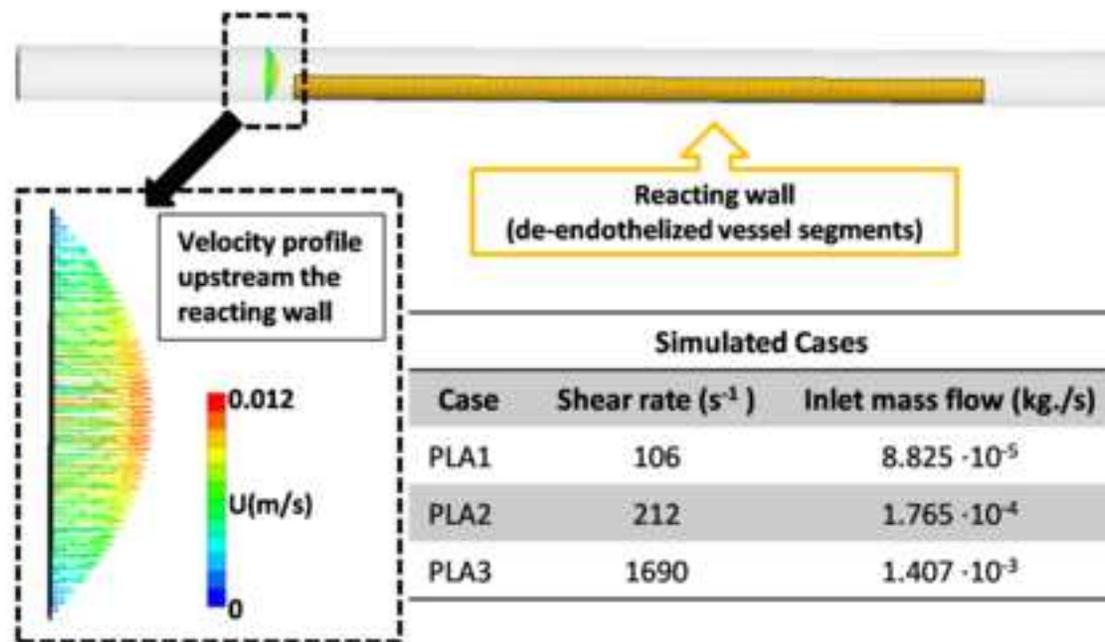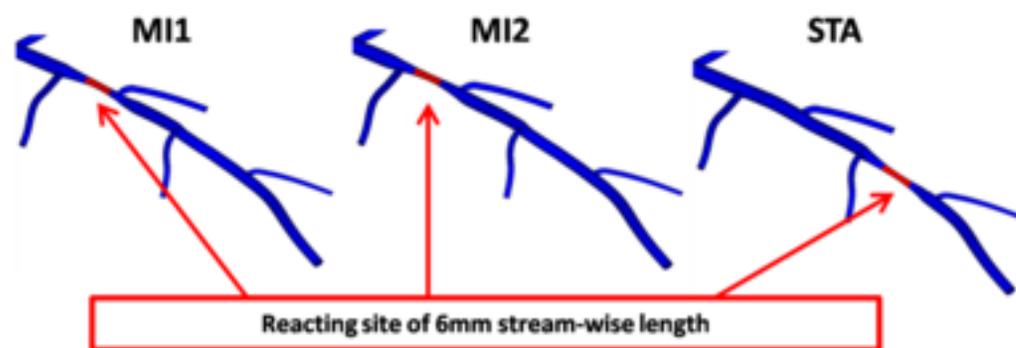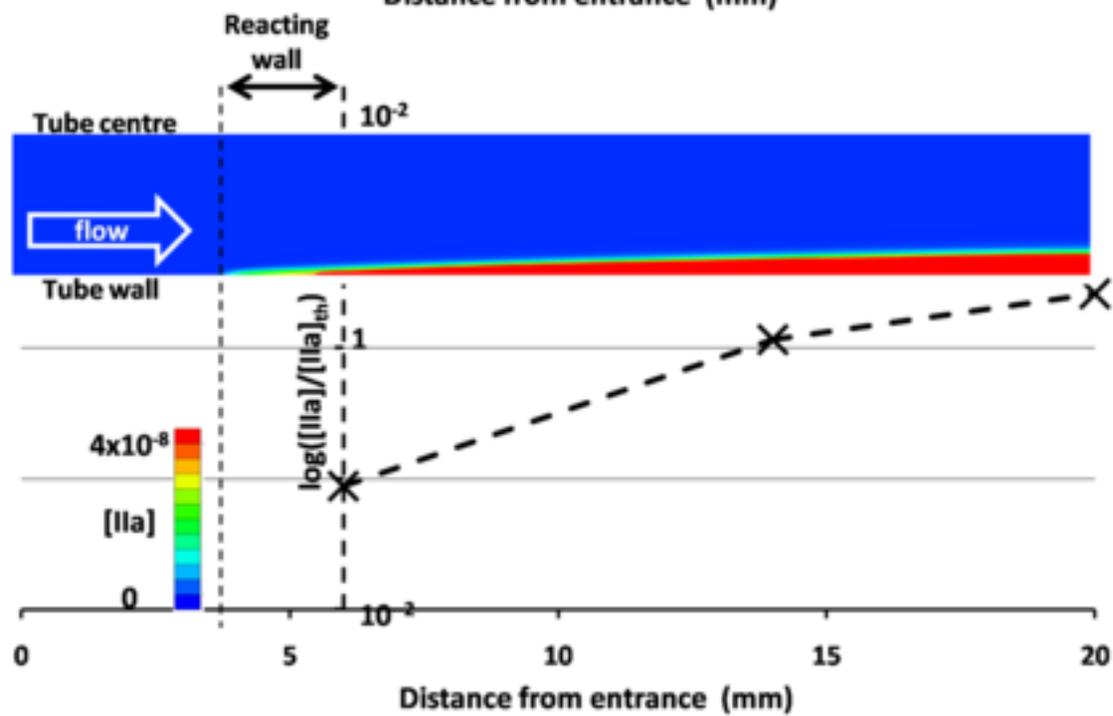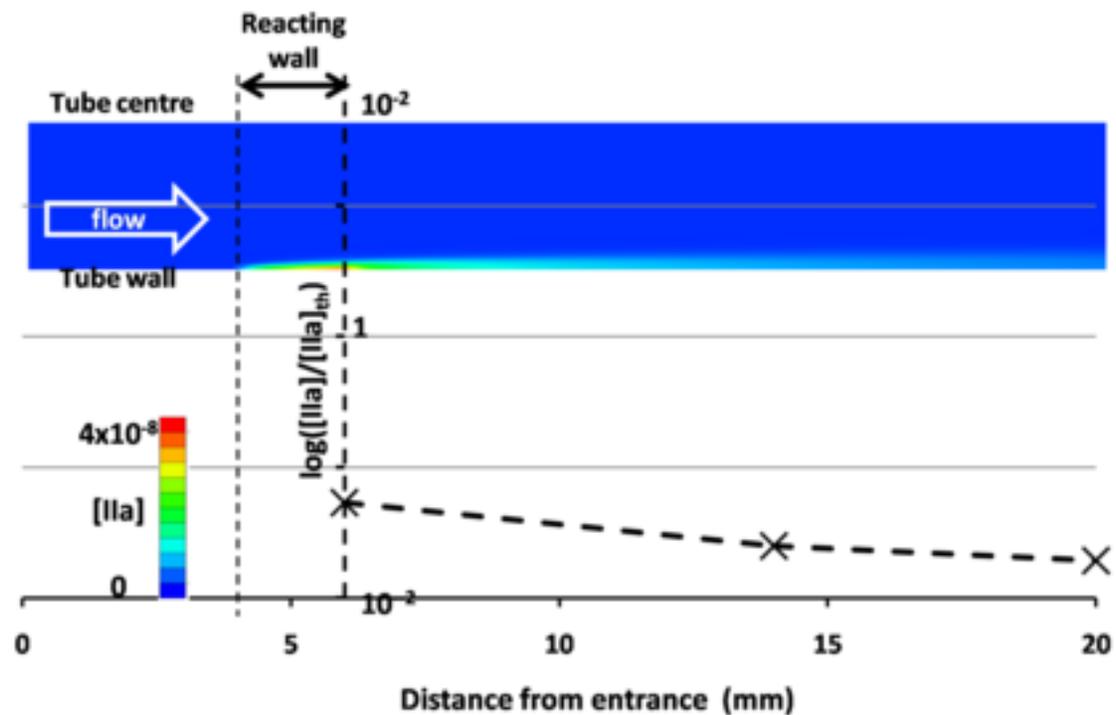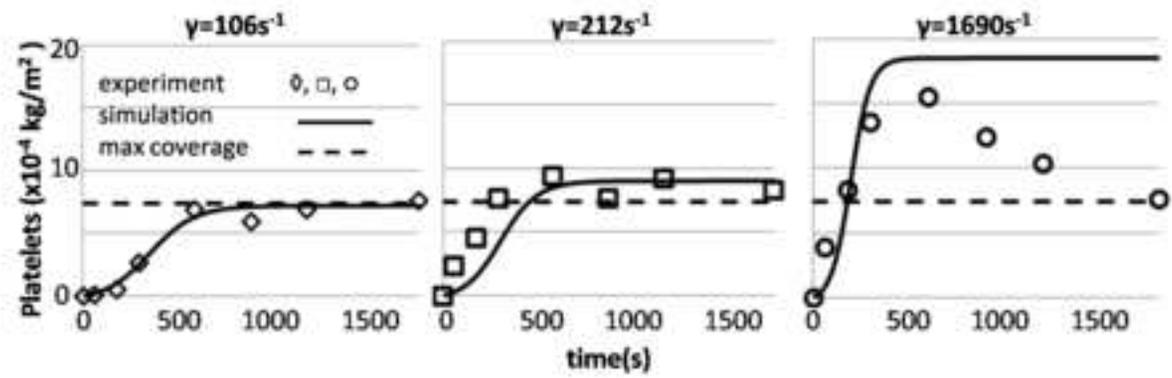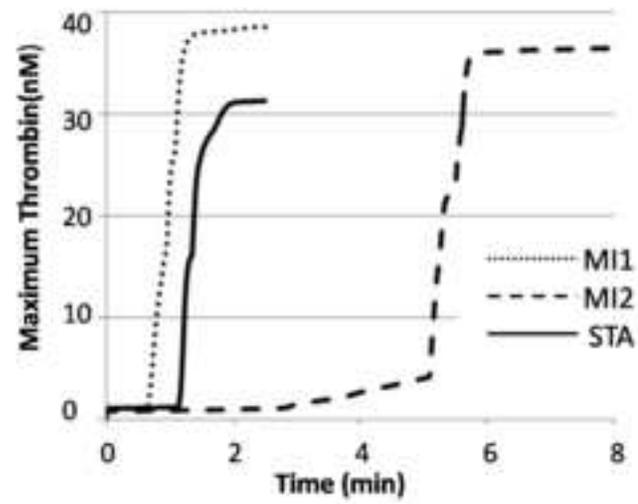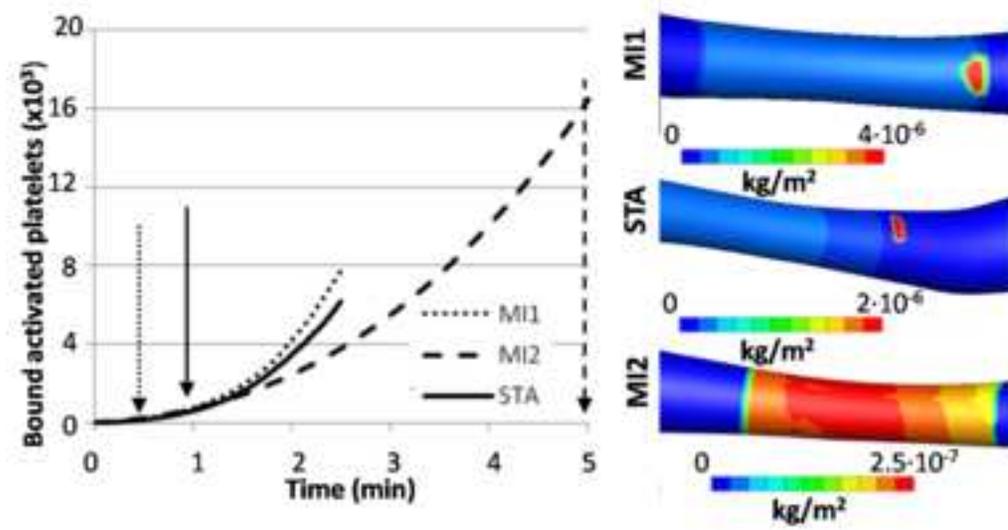
Supplementary data

Click here to download Supplementary data: Appendix.docx